ACS Catalysis

pubs.acs.org/acscatalysis

Research Article

In-Situ-Generated Active Hf-hydride in Zeolites for the Tandem N-Alkylation of Amines with Benzyl Alcohol

Sergio Rojas-Buzo, Patricia Concepción, Avelino Corma, Manuel Moliner,* and Mercedes Boronat*

Cite This: *ACS Catal.* 2021, 11, 8049−8061

Read Online

ACCESS | Metrics & More | Article Recommendations | Supporting Information

ABSTRACT: In this work, we have studied the catalytic activity of different silicates (MFI, MCM-41, and Beta) containing Lewis acid sites (including Sn, Ti, Zr, and Hf) for the tandem N-alkylation reaction of aniline with benzyl alcohol. The Hf- and Zr-Beta were the most active catalysts for this transformation, showing in both cases selectivities toward the corresponding *N*-benzylaniline higher than 97%. FTIR and DFT analyses confirm that the active sites in the Hf-Beta catalyst for this process are the open sites where one of the four Hf−O bonds is hydrolyzed. Moreover, the amount of these active species could be notoriously increased with previous thermal treatment of the Lewis acid zeolite with benzyl alcohol. Isotopically labeled experiments and theoretical mechanistic studies reveal that the N-alkylation reaction occurs through a hydrogen borrowing pathway, in which *in situ* Hf-hydride species were generated. Finally, the Hf-Beta zeolite was reused several times in the N-alkylation reaction without any appreciable deactivation detected. This catalytic system could be expanded to a variety of amines, including aliphatic and biomass-derived amines.

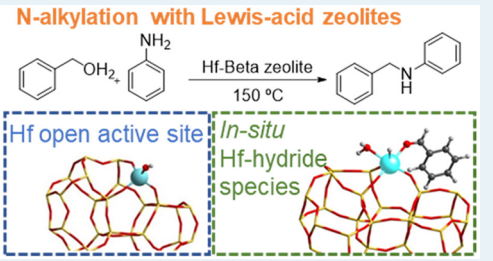

KEYWORDS: *zeolites, Lewis acid, open site, N-alkylation, Hf-hydride*

1. INTRODUCTION

Transition-metal hydrides have been recognized for many years as intermediates or catalysts in industrially relevant processes, such as hydroformylation, olefin isomerization, or hydrogen exchange in alkanes, among others.[1] Since 1955, when the first organometallic transition-metal hydride was discovered ($(Cp)_2ReH$),[2] the discipline of organometallic chemistry has exponentially grown. A common strategy to *in situ* generate reactive transition-metal hydrides is via a borrowing hydrogen (BH) approach from a donor molecule.[3] The borrowing hydrogen methodology, also called hydrogen autotransfer, is a powerful strategy that combines transfer hydrogenation with one or more intermediate reactions, avoiding the direct use of molecular hydrogen. The key of this concept is that the hydrogen from a donor molecule is stored by a catalytic metal site to be released in a final hydrogenation step.[3] This approach has been tentatively applied in the tandem N-alkylation reaction of amines using alcohols as hydrogen donors and either noble-metal-based (i.e., Ru, Pd, Ir, Rh, and Au)[4−8] or, more recently, non-noble transition metals (i.e., Mn, Co, Ni, and Fe)[9−12] complexes as catalysts. However, these homogeneous catalytic systems present some important drawbacks, mainly related to the recovery and reuse of expensive catalysts and/or the indispensable use of bases to deprotonate the alcohol. The principal heterogeneous catalysts that have been reported for this transformation consist of transition-metal sites supported on inorganic materials[13−16] or metal nanoparticles.[17] However, these solids still present some key disadvantages, including metal leaching and/or uncertain stability and recyclability.

Group 4 transition-metal-hydride-based heterogeneous catalysts have attracted much less attention. Despite this, homogeneous hafnium and zirconium complexes, bearing cyclopentadienyl ligands $(Cp)_2M(H)R$, have been extensively studied and utilized in diverse chemical processes, such as N_2 reduction, hydrogenolysis, and transmetalation reactions.[18,19] These systems not only show limitations associated with catalyst recyclability but also suffer from deactivation in open atmospheres. Few studies on grafting isolated single Hf and Zr sites on highly stable inorganic supports have been reported.[20−23] Based on the reaction of alkyl metal complexes with dehydroxylated silica surfaces and the subsequent hydrogen treatment, well-defined mono- and bishydrides have been anchored on silica support.[20] These Hf- and Zr-hydrides are reactive under mild reaction conditions for different alkane transformations.[21−23] However, in all these cases, inert atmospheres are necessary to prevent M−H deactivation. Moreover, it is worth noting that, as far as we know, the efficient N-alkylation of amines with alcohols has

Received: April 19, 2021
Revised: June 3, 2021

https://doi.org/10.1021/acscatal.1c01739
ACS Catal. 2021, 11, 8049−8061

not been reported using isolated Zr and Hf sites, neither in homogeneous nor heterogeneous catalysts.

Having this target in mind, we propose to study the potential ability of the isolated Hf and Zr sites in high-silica zeolites to generate *in situ* metal-hydride species. In this sense, isolated sites of different transition metals (including Ti, Sn, Zr, and Hf) have been incorporated in framework positions of different silicate matrixes (Beta, MFI, and MCM-41). The diverse metal-containing materials have been characterized using UV−vis spectroscopy to demonstrate the full incorporation of the Lewis acid sites in framework positions. The Lewis-acid-containing zeolites have been found to be active for the N-alkylation reaction of aniline using benzyl alcohol as a hydrogen donor, where Hf- and Zr-Beta show the best catalytic performance, giving the corresponding *N*-benzylaniline product with high selectivity. Kinetic studies reveal an induction period when using Hf-Beta as a catalyst that can be suppressed if a previous activation with benzyl alcohol is performed. DFT calculations and FTIR analysis indicate that tetrahedral Hf sites in Beta zeolite must be in the open form, that is, with one of the four Hf−O bonds hydrolyzed, to catalyze the dehydrogenation of benzyl alcohol to benzaldehyde, being the amount of open sites considerably higher after a continuous exposure of the Hf-Beta zeolite to the alcohol. Moreover, theoretical and experimental mechanistic studies reveal that the process occurs through hydrogen borrowing from the methylene group present in benzyl alcohol. Finally, Hf-Beta has demonstrated high stability in this transformation, since it could be reused at least four times without appreciable deactivation. The catalytic system can be extended to the use of aliphatic and biomass-derived amines.

2. EXPERIMENTAL SECTION

2.1. Synthesis. *2.1.1. Synthesis of Zr-DeAl-Beta.* Commercially available Al-Beta (1 g, CP814E) was dealuminated with 25 mL of HNO_3 (65%) at 80 °C for 16 h under magnetic stirring. After filtration and washing with abundant water, the resulting solid was dried at 170 °C overnight. Afterward, zirconium was grafted as follows: $ZrOCl_2{\cdot}8H_2O$ (46.8 mg, 0.14 mmol) was dissolved in ethanol (80 mL). The resulting ethanolic solution was added dropwise to the activated dealuminated Beta. Then, the resulting mixture was refluxed under magnetic stirring at 100 °C for 5 h. After washing with ethanol, the white solid obtained was dried at 100 °C prior to calcination at 550 °C in air for 6 h.

2.1.2. Synthesis of Zr-MFI. First, $ZrCl_4$ (29.3 mg, 0.13 mmol) was dissolved in water (0.85 g). The resulting aqueous solution was magnetically stirred, while TEOS (3.48 g) was added dropwise. When homogeneous gel was obtained, a solution of TPAOH (40 wt %, 2.96 g) in water (5.16) was incorporated. After 1 h under stirring, water (2.80 g) was added, resulting in the following molar composition gel: 1 SiO_2/0.0075 ZrO_2/0.35 TPAOH/35.2 H_2O. The final gel was left overnight under magnetic stirring. Then, ethanol formed from the hydrolysis of TEOS was evaporated at room temperature for 2 h. The gel was subjected to crystallization in a Teflon-lined stainless-steel autoclave at 150 °C for 5 days. The solid obtained was filtered and washed with water, dried at 100 °C, and calcined at 550 °C in air for 4 h.

2.1.3. Syntheses of M-Beta. M-Beta zeolites with Si/M between 50 and 155 were synthesized as follows: first, tetraethylammonium hydroxide solution (35 wt % in water) was mixed with tetraethyl orthosilicate (TEOS) in a polytetrafluoroethylene (PTFE) jar. This mixture was allowed to stir at room temperature for 90 min. Then, an aqueous solution of the corresponding metal salt was added, and the mixture was left to stir until the ethanol formed upon hydrolysis of TEOS was evaporated. Hydrofluoric acid was added under vigorous stirring until a thick gel was formed. Finally, 5 wt % (silica basis) of dealuminated Beta was added as seed crystals. The final gel composition was 1 SiO_2/*x* MO_2/0.56 TEAOH/0.56 HF/7.5 H_2O. The gels were transferred to Teflon-lined stainless-steel autoclaves and, then, placed in an oven at 140 °C for the required time to crystallize the M-Beta zeolites under static conditions. The resulting solids were filtrated and extensively washed with water. The M-Beta samples were dried at 100 °C and, finally, calcined at 550 °C in air for 4 h.

2.1.4. Synthesis of Zr-MCM-41. In a typical synthesis, C_{16}TMABr (4.55 g) was dissolved in water (30.5 g) at 40 °C until a clear solution was obtained. Then, the solution was cooled down to room temperature and TMAOH solution (25 wt %, 7.88 g) and $ZrOCl_2{\cdot}8H_2O$ (2.67 g) were added, and the resulting mixture was stirred for 5 min. Finally, SiO_2 Aerosil (5 g) was added. The homogeneous mixture was stirred at room temperature for 1 h and, subsequently, heated at 135 °C for 24 h in a Teflon-lined stainless-steel autoclave without rotation. The as-prepared Zr-MCM-41 sample was recovered by filtration and extensively washed with distilled water (2 L/g solid), and then, the material was dried at 100 °C overnight. The occluded surfactant was removed by heating the sample at 540 °C under a continuous flow of N_2 for 1 h, followed by 6 h in a flow of air at the same temperature.

2.2. Characterization Techniques. Powder X-ray diffraction (PXRD) measurements were performed using a Panalytical CubiX diffractometer operating at 40 kV and 35 mA and using Cu Kα radiation (λ = 0.1542 nm).

Chemical analyses were carried out in a Varian 715-ES ICP-Optical Emission spectrometer, after solid dissolution in HNO_3/HCl/HF aqueous solution.

The morphology of the samples was studied by field emission scanning electron microscopy (FESEM) using a ZEISS Ultra-55 microscope.

The UV−vis spectra were collected using an Agilent Cary 7000 UV−vis−NIR spectrophotometer equipped with a diffuse reflectance accessory.

Raman spectra were recorded with an inVia Renishaw spectrometer equipped with an Olympus microscope. The samples were excited by the 325 nm line of a He−Cd laser (Kimmon) with a laser power of 20 mW.

2.3. Computational Details. All density functional theory (DFT) calculations were carried out using the M062X functional,[24] the 6-31g(d,p) basis set for O, C, N, and H atoms,[25,26] and the LANL2DZ basis set and pseudopotential for Hf,[27,28] as implemented in the Gaussian09 software.[29] The active sites in Hf-Beta were simulated by cluster models cut out from the periodic crystalline structure of Beta zeolite and containing one framework Hf atom at the T9 position bonded to four −O−Si units (closed site) or with one hydrolyzed Hf−OH bond (open site). The dangling bonds that connected the cluster with the rest of the solid were saturated with H atoms, and during geometry optimizations, these terminal H atoms were kept fixed to maintain the zeolite structure, while all other atoms in the model were allowed to relax without restrictions. All stationary points were characterized by frequency calculations, which also provided the zero-point vibrational

https://doi.org/10.1021/acscatal.1c01739
ACS Catal. 2021, 11, 8049−8061

corrections to the energy (ZPE). Activation E_{act} and reaction ΔE energies for each elementary step were calculated as

$$E_{act} = E(TS) - E(R)$$

$$\Delta E = E(P) - E(R)$$

Where $E(R)$, $E(TS)$, and $E(P)$ are the total energies of the reactant, transition state, and product structures, respectively. Net atomic charges were obtained using the natural bond order (NBO) analysis[30] as implemented in Gaussian 09 software.

2.4. FTIR Analysis. IR spectra were recorded with a Thermo is50 FTIR spectrometer using a DTGS detector and acquired at 4 cm^{-1} resolution. A homemade quartz IR cell allowing *in situ* treatments in controlled atmospheres and temperatures from 25 to 525 °C has been connected to a vacuum system with gas dosing facility.

For IR studies, the samples were pressed into self-supported wafers and treated at 300 °C in vacuum (10^{-4} mbar) for 2 h. After activation, the samples were cooled down to 100 °C under dynamic vacuum conditions followed by benzyl alcohol dosing at 0.5 mbar and subsequent evacuation. Then, the temperature was increased under dynamic vacuum conditions up to 150 °C, kept at that temperature for 2.5 h, and cooled down to 100 °C, when benzyl alcohol was added for a second time. IR spectra were recorded at each step. In the *in situ* studies, at this step, aniline was coadsorbed at 1 mbar, followed by evacuation and increasing the temperature to 100 °C, keeping at the same temperature for 30 min.

For IR experiments of acetonitrile (CD_3CN) titration, in the case of the fresh sample, it has been activated at 300 °C in vacuum for 2 h and then cooled down to 25 °C, followed by CD_3CN dosing at 2 mbar. In the case of the benzyl alcohol treatment at 150 °C for 2 h, the sample was cooled down to 100 °C under dynamic vacuum followed by CD_3CN dosing at 2 mbar.

2.5. Catalytic Tests. *2.5.1. N-Alkylation of Aniline with Benzyl Alcohol Using Lewis-Acid-Containing Silicates as a Catalyst.* Reactions were performed in 2 mL glass-vessel reactors equipped with a magnetic bar. A solution of aniline (74.1 mg, 0.8 mmol), benzyl alcohol (86.9 mg, 0.8 mmol), and dodecane (35.6 mg, 0.2 mmol), used as an internal standard, in *o*-xylene (1.8 mL) was added to each reactor containing the corresponding amount of catalyst (50:1 substrate:/metal molar ratio). The mixtures were heated up at 150 °C and left to stir for 4.5 h. Approximately 25 μL of aliquots was taken, diluted with 1 mL of ethyl acetate, and filtered with a PTFE syringe filter.

Gas chromatographic analyses were performed in an instrument equipped with a 25 m capillary column of 5% phenylmethylsilicone using dodecane as an internal standard unless otherwise indicated. The method employed for the analysis starts at 100 °C with a ramp of 20 °C/min until achieving 280 °C, which is maintained for 2 additional minutes. GC−MS analyses were performed on a spectrometer equipped with the same column as the GC and operated under the same conditions to identify the products.

2.5.2. N-Alkylation of Aniline with Benzyl Alcohol as a Solvent. Reactions were performed in 2 mL glass-vessel reactors equipped with a magnetic bar. A solution of aniline (0.8 mmol) and dodecane (35.6 mg, 0.2 mmol) in benzyl alcohol (1.8 mL) was added to the reactor containing 125 mg of Hf-Beta (50:1 amine/Hf molar ratio). The mixture was heated up at 150 °C and left to stir during the required time. Approximately 25 μL of aliquots was taken, diluted with 1 mL of ethyl acetate, and filtered with a PTFE syringe filter. Benzyl alcohol activation was performed as follows: benzyl alcohol (1.8 mL) was added to the reactor containing 125 mg of Hf-Beta (50:1 amine/Hf molar ratio). The mixture was heated up at 150 °C and left to stir during 4 h. After that period, aniline and dodecane were injected, and the reaction was followed with time.

2.5.3. General Procedure for the N-Alkylation of Amines with Alcohols. Reactions were performed in 2 mL glass-vessel reactors equipped with a magnetic bar. A solution of amine (0.4 mmol) and dodecane (17.8 mg, 0.1 mmol) in the corresponding alcohol (0.9 mL) was added to each reactor containing 62.5 mg of Hf-Beta (50:1 amine/Hf molar ratio). The mixtures were heated up at 150 °C and left to stir during the corresponding time. Approximately 25 μL of aliquots was taken, diluted with 1 mL of ethyl acetate, and filtered with PTFE syringe filter.

2.5.4. Mechanistic Experiments. Reactions with isotopically labeled benzyl alcohol in different positions were performed in a 2 mL glass-vessel reactors equipped with a magnetic bar. A solution of aniline (18.5 mg, 0.2 mmol) and benzyl alcohol (0.2 mmol) in *o*-xylene (0.45 mL) was added to each reactor containing 31 mg of Hf-Beta (50:1 substrate/Hf molar ratio). The mixtures were heated up at 150 °C and left to stir for 4.5 h. The reaction mixtures were quenched with ice, filtered with a PTFE syringe filter, and diluted with toluene-d_8. Afterward, the solutions were analyzed by ^{1}H NMR spectroscopy.

Benzyl alcohol-OD was prepared following a previous report in the literature.[31] Benzyl alcohol was magnetically stirred with an excess of deuterium oxide for 1 h, followed by extraction with diethyl ether, drying with anhydrous magnesium sulfate, and solvent evaporation.

^{1}H NMR was recorded on a Bruker 300 spectrometer at a spinning rate of 15 kHz with a 90° pulse length of 5 μs using high-power proton decoupling (spinal64) μs with a 20 s repetition time, and the chemical shifts are reported in ppm relative to residual proton solvent signals.

2.5.5. Reuse Study. Following the alcohol activation process, after a typical N-alkylation reaction between aniline and benzyl alcohol, Hf-Beta was separated from the reaction medium by centrifugation and, then, washed with ethyl acetate and dichloromethane. After that, the solvent was evacuated under vacuum at room temperature prior to the utilization in the next run.

3. RESULTS AND DISCUSSION

3.1. Synthesis of M-Silicates and Their Catalytic Evaluation for the N-Alkylation of Aniline with Benzyl Alcohol. Group 4 transition metal sites can be incorporated in high-silica zeolites in dilute amounts, generating M^{IV} isolated atoms with unique Lewis acid properties.[32−36] In order to study if these M-zeolites could act as adequate alternative catalysts for the base-free N-alkylation reaction of amines with alcohols, we have initially incorporated different transition metals (including Ti, Sn, Zr, and Hf) in framework positions of a large-pore Beta zeolite (see Experimental Section).

The PXRD patterns of each material show the characteristic diffractogram of the crystalline Beta phase (see Figure S1). The ICP analyses of the different metal-containing Beta zeolites, M-Beta, synthesized in fluoride media, present Si/M molar ratios of ∼130−150 (see Zr-, Hf-, and Sn-Beta in Table S1), except

https://doi.org/10.1021/acscatal.1c01739
ACS Catal. 2021, 11, 8049−8061

Scheme 1. N-Alkylation of Aniline with Benzyl Alcohol Catalyzed by Different Metal-Containing Silicates

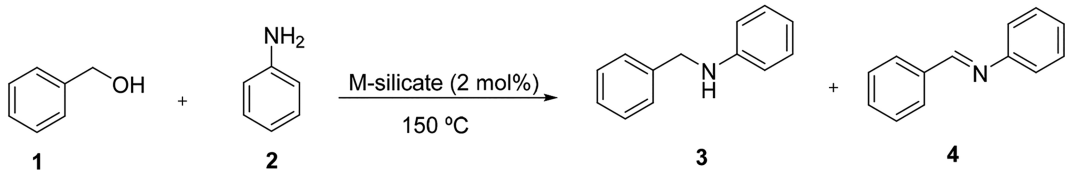

for Ti-Beta, which presents a lower Si/M molar ratio (Si/Ti ≈ 50, see Ti-Beta in Table S1). UV−vis spectra of the calcined M-Beta zeolites suggest in all cases the presence of tetrahedrally coordinated isolated metallic species, as revealed by the single signal centered between 190 and 230 nm (see Figure S2a). Moreover, the UV Raman spectra of all Lewis-acid-containing Beta zeolites show a band centered at ∼696 nm that is not present in the Si-Beta spectrum and that is assigned to M atoms incorporated in the Beta framework (see Figure S2b).[37,38] The oxide phase is not observed in any M-Beta zeolites' Raman spectra (see Figure S2b), so taking into account the detection limit of Raman spectroscopy, these samples do not contain extra-framework MO_2 species. Finally, the average particle sizes of the different M-Beta zeolites are 1−3 μm (see FE-SEM images in Figure S3).

For comparison purposes, other Zr-containing silicates have also been prepared, including a nanosized Zr-Beta zeolite, a medium-pore Zr-MFI, and a mesoporous Zr-MCM-41 (see Experimental Section for details).[39−41] Despite these comparative materials presenting different Si/Zr molar ratios (see Table S1), UV−vis spectra reveals that most of the Zr species in these silicates have been incorporated as isolated species (see Figure S2).

At this point, the above prepared Lewis-acid-containing silicates have been tested as catalysts for the N-alkylation of aniline **2** with benzyl alcohol **1** in equimolar conditions using *o*-xylene as a solvent (see Scheme 1).

A blank experiment without a catalyst has been first evaluated (Table 1, entry 1), where neither *N*-benzylaniline **3** nor the corresponding *N*-benzylideneaniline **4** are detected by gas chromatography after 4.5 h. Among the different M-silicates, Zr- and Hf-containing Beta zeolites show the highest catalytic activity and selectivity toward formation of the secondary amine **3** (Table 1, entries 2 and 3, respectively). In both cases, only traces of the corresponding imine **4** have been detected as a byproduct.

Table 1. N-Alkylation of Aniline with Benzyl Alcohol Using Lewis-Acid-Containing Silicates as Catalysts at 150 °C for 4.5 h

entry	catalyst	X_1 (%)[a]	X_2 (%)[b]	S_3 (%)[c]	S_4 (%)[d]
1	-	0	0	n.d.	n.d.
2	Zr-Beta	96.1	95.5	97.7	1.6
3	Hf-Beta	95.7	95.4	97.2	2.3
4	Sn-Beta	6.3	7.1	46.6	22.3
5	Ti-Beta	3.2	3.7	25.2	34.0
6	Zr-MFI	3.5	3.8	55.5	53.3
7	Zr-MCM-41	4.9	4.1	n.d.	18.9
8	Zr-DeAl-Beta	17.5	16.1	67.1	8.4
9	Al-Beta	12.5	12.7	42.6	10.7

[a]Benzyl alcohol conversion. [b]Aniline conversion. [c]*N*-Benzylaniline selectivity. [d]*N*-Benzylideneaniline selectivity.

Other Lewis-acid-containing Beta zeolites, such as Sn- and Ti-Beta, only give the desired product **3** in low yields and selectivities, with appreciable amounts of imine **4** being detected in both cases (Table 1, entries 4 and 5 respectively). This dissimilar catalytic behavior offered by the different metals could be first tentatively assigned to their Lewis acid strength,[42] which has been reported to follow the subsequent order: Ti < Sn < Zr, in concordance with our experimental observations for this reaction.

The influence of the pore size accessibility for the N-alkylation reaction exposed above has been evaluated with the Zr-silicates presenting different pore sizes (Zr-MFI and Zr-MCM-41) and crystal sizes (Zr-DeAl-Beta). The medium-pore-size Zr-MFI shows much lower catalytic activity than Zr-Beta (Table 1, entries 6 and 2, respectively), suggesting that the product formation would have steric impediments within the smaller channels of the MFI structure compared to Beta (5−5.5 and 6.5−7 Å, respectively). In contrast, Zr-MCM-41, with a pore size of 2−3 nm, is not able to produce the desired *N*-benzylaniline product after 4.5 h (Table 1, entry 7). In this case, limited diffusion pathways cannot be claimed, but the combination of a very hydrophilic surface and the absence of tight molecular confinements within the mesoporous channels could be two interconnected plausible reasons explaining the poor catalytic activity offered by the Zr-MCM-41 catalyst. The highly accessible Zr-DeAl-Beta shows a remarkably lower conversion and selectivity toward **3** than regular Zr-Beta (Table 1, entries 8 and 2, respectively), even when the nanosized Beta sample shows a significant lower particle size (30 nm and 1 μm for Zr-DeAl-Beta and Zr-Beta, respectively, see Figure S3). This result also suggests that the high hydrophilicity encountered when the particle size is reduced to a few nanometers would be responsible for the low catalytic activity observed when using Zr-DeAl-Beta as a catalyst. Finally, a commercially available Beta zeolite containing Brønsted acid sites (CP814E, Zeolyst) has also been evaluated, but under the selected reaction conditions, only 12% conversion with 43% selectivity toward *N*-benzylaniline was observed (Table 1, entry 9). The results achieved with Al-Beta indicate the limited ability of Brønsted acid sites to properly catalyze the N-alkylation reaction between aniline and benzyl alcohol.

3.2. Activation of Hf-Beta with Benzyl Alcohol: Increasing Catalytically Active Lewis Open Sites. The N-alkylation of aniline with benzyl alcohol using *o*-xylene as a solvent was followed over time using Hf-Beta as a catalyst and varying the ratio between benzyl alcohol and aniline. If an excess of aniline is employed (4 equiv of aniline per benzyl alcohol), the achieved conversion values are below 10% with poor selectivities to *N*-benzylaniline after 4.5 h at 150 °C (below 30%, see blue triangles in Figure S4). In contrast, excellent yield to *N*-benzylaniline is observed after 4.5 h and 150 °C when using equimolar quantities of aniline and benzyl alcohol (∼95%, see black squares in Figure S4-right), but the

https://doi.org/10.1021/acscatal.1c01739
ACS Catal. 2021, 11, 8049−8061

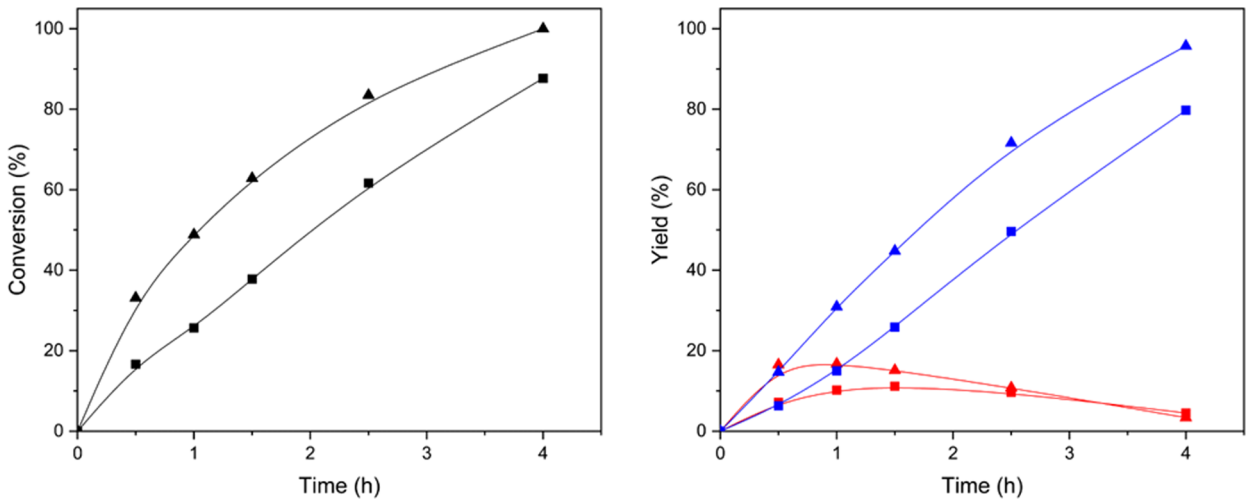

Figure 1. Conversion (black lines) and yield of **3** (blue lines) and **4** (red lines) obtained for the N-alkylation of aniline with benzyl alcohol using fresh Hf-Beta (squares) and Hf-beta activated previously with benzyl alcohol (triangles) as catalyst. Reaction conditions: aniline (0.8 mmol) in benzyl alcohol (1.8 mL). The mixture was heated up at 150 °C and left to stir during the corresponding time. Dodecane was employed as an internal standard. Hf-Beta (50:1 aniline/metal molar ratio).

kinetic curve clearly reveals the presence of an initial induction period of ∼3 h (see black squares in Figure S4-left). Interestingly, this initial induction period is considerably softened when adding an excess of benzyl alcohol in the reaction media (4 equiv of benzyl alcohol per aniline, see red circles in Figure S4-left), achieving high *N*-benzylaniline yield after 4.5 h (∼90%, see red circles in Figure S4-right). These preliminary results suggest that benzyl alcohol would have an important role in the N-alkylation reaction mechanism and/or in the activation of the Hf-Beta active sites.

To better understand the effect of benzyl alcohol, additional experiments have been carried out using Hf-Beta as a catalyst and benzyl alcohol not only as an alkylation agent but also as reaction solvent under the same reaction conditions as those described above (see Experimental Section). The reaction has been first studied using fresh Hf-Beta as a catalyst (see squares in Figure 1). The conversion at 0.5 h shows a 2-fold increase when using benzyl alcohol as a solvent (∼17%, see square at 0.5 h in Figure 1-left) compared to the previous experiment using a few equivalents of benzyl alcohol in *o*-xylene (∼8%, see red circle at 0.5 h in Figure S4-left). In terms of product yields, imine **4** and *N*-benzylaniline **3** are detected in equimolar quantities at low reaction times (∼8−9%, see red and blue squares respectively at 0.5 h in Figure 1-right). Afterward, imine **4** disappears with time, while the secondary amine shows a continuous increase, finally obtaining the desired *N*-benzylaniline product with high yields after 4 h (80%, see blue square at 4 h in Figure 1-right).

Recently, it has been reported that a previous aging of a Hf-Beta catalyst with methanol allows increasing the catalytic performance of this material for the glucose isomerization reaction.[43] Despite there not being a definitive explanation for this improvement, it would not be surprising that methanol could modify the nature of the isolated Lewis acid active sites (i.e., increasing the amount of Hf open sites). Thus, the remarkable catalytic activity enhancement achieved here when increasing the benzyl alcohol amount from equimolar contents to a substantial excess in the reaction media would suggest that the Hf-Beta active sites required to efficiently undergo the N-alkylation reaction could be influenced by benzyl alcohol.

Thus, an additional experiment has been performed where Hf-Beta has been activated with benzyl alcohol for 4 h at 150 °C, and after that period, the corresponding amount of aniline has been injected in the mixture and the reaction allowed to proceed. The catalytic activity has increased considerably after the previous activation step (see black triangles in Figure 1-left). Moreover, after 4 h, the conversion achieved is complete, with a product yield toward **3** higher than 95% (see blue triangle at 4 h in Figure 1-right). This experiment undoubtedly confirms that benzyl alcohol allows activating Hf-Beta sites for the N-alkylation reaction.

To shed light on the nature of the isolated Lewis acid sites before and after benzyl alcohol activation, two *in situ* IR studies have been designed. On the one hand, benzyl alcohol has been directly added at 100 °C on the fresh Hf-Beta sample (see Figure 2a), and on the other hand, Hf-Beta has been exposed to the alcohol at 150 °C for a period of 2.5 h, followed by evacuation and cooling down to 100 °C (Figure 2b) (see

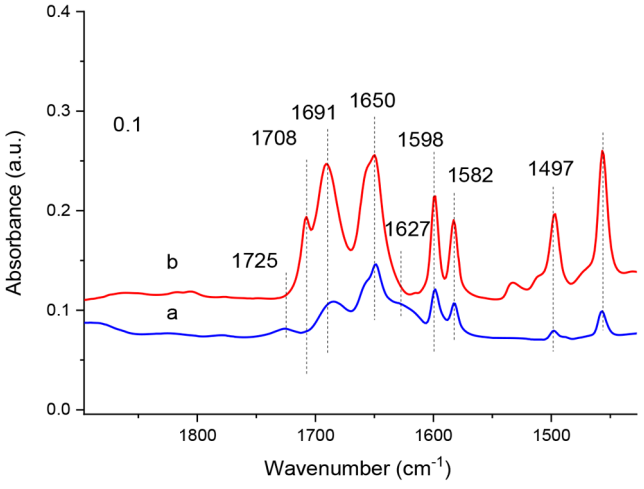

Figure 2. IR spectra of 0.5 mbar of benzyl alcohol adsorbed at 100 °C on (a) a fresh Hf-Beta sample and (b) after having been exposed at 150 °C to the alcohol for a period of 2.5 h followed by evacuation and cooling down to 100 °C.

https://doi.org/10.1021/acscatal.1c01739
ACS Catal. 2021, 11, 8049−8061

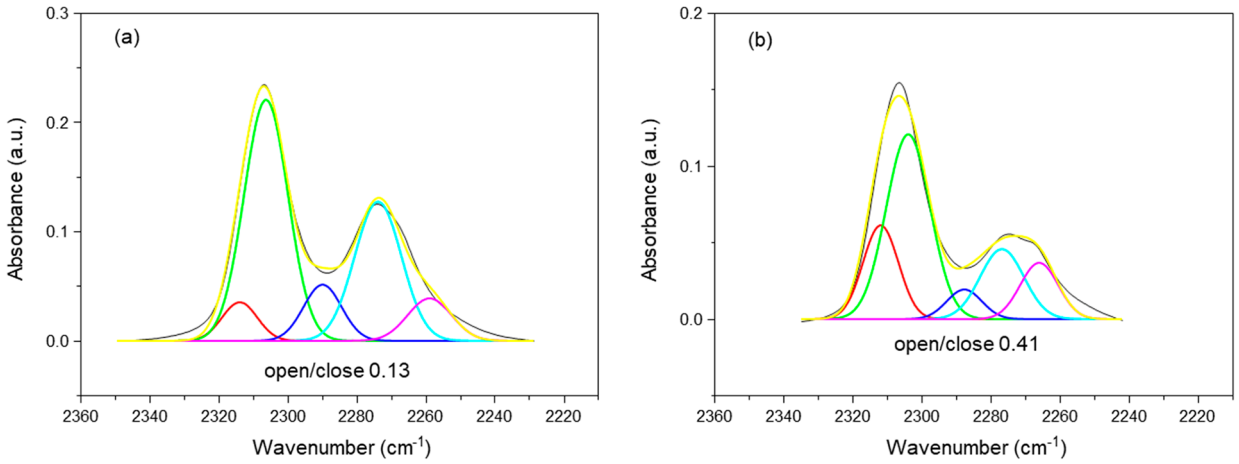

Figure 3. IR deconvoluted spectra of 2 mbar of CD_3CN adsorbed at 25 °C on (a) a fresh Hf-Beta sample and (b) after having been exposed at 150 °C to benzyl alcohol for a period of 2.5 h. The IR bands at 2312 and 2306 cm^{-1} are associated with CD_3CN coordinated to Hf sites, and the IR bands at 2287, 2276, and 2264 cm^{-1} are associated with OH groups in the Beta zeolite.

Experimental Section for details). As observed, benzaldehyde is formed in both cases characterized by a set of IR bands at 1691, 1650, 1598, and 1582 cm^{-1} (C=O, aromatic, and CH vibration, respectively) of adsorbed species. The band at 1725 cm^{-1} might be related to Hf−H species, due to hydride abstraction resulting in aldehyde formation, and the shoulder at 1627 cm^{-1} is due to δ(O−H) of water forming according to the mechanism described in the DFT studies. Aldehyde formation increases markedly once the sample is pre-exposed to benzyl alcohol at 150 °C with the detection of gas phase aldehyde species (IR at 1708 cm^{-1}).

Finally, an additional experiment using isotopically enriched $PhCD_2OH$ was carried out in order to confirm the assignment of the Hf−H bond by isotopic Hf−D substitution. As observed in Figure S5, the IR band at 1725 cm^{-1}, associated with Hf−H, is not present when using deuterated alcohol at the same time that the band associated with C=O vibration (1691 cm^{-1}) is shifted to lower frequencies due to the isotopic exchange (1674 cm^{-1}). Additional DFT calculations have been performed, and values of 1770 and 1256 cm^{-1} have been obtained for the ν(Hf−H) and ν(Hf−D) stretching frequencies, respectively. According to these calculations, the Hf−D stretching vibration is expected to appear around 1200 cm^{-1}, the region where the detector is saturated due to (Si−O−Si) vibrations. The rest of the bands remain in practically the same position, while some of them present with lower intensity (see Figure S5).

Previous work has shown that the closed sites in Sn-Beta zeolite transform into open sites with one hydrolyzed bond under ethanol dehydration reaction conditions.[44] To confirm whether the benzyl alcohol thermal treatment produces the same transformation of active sites in Hf-Beta zeolite, the open and closed sites in nonactivated and activated Hf-Beta samples have been characterized by *in situ* IR spectroscopy using deuterated acetonitrile CD_3CN as a probe molecule. According to previous assignments on Sn-Beta samples[33,45] and present DFT simulations, a larger shift in the ν(C≡N) IR band should be expected for acetonitrile adsorbed on hydrolyzed or open Hf sites (see Figure S6). Thus, the IR spectra of CD_3CN adsorbed on the fresh Hf-Beta (Figure 3a) and on a Hf-Beta after being exposed *in situ* to benzyl alcohol at 150 °C for 2.5 h (Figure 3b) show two bands at 2312 and 2306 cm^{-1}, corresponding to the open and closed sites, respectively. Interestingly, the amount of open sites increases in the Hf-Beta sample after being exposed to benzyl alcohol at 150 °C, as indicated by the open/closed ratios, 0.13 in the fresh sample vs 0.41 in the sample treated with benzyl alcohol. The fact that the aldehyde formation is enhanced in the treated sample confirms that the open sites are the catalytically active sites for this reaction and that they are generated under alcohol exposure at 150 °C, explaining in this way the removal of the induction period observed in the catalytic study.

3.3. N-Alkylation Reaction Mechanism: Theoretical and Experimental Mechanistic Studies. Once the nature of the active sites in Hf-Beta has been established by catalyst testing and IR spectroscopy, the complete reaction mechanism has been studied by means of DFT calculations on an open site model, as described in the Computational Details section. This model contains the Hf Lewis acid site and a basic hydroxyl group able to accept a proton and produce water that remains coordinated to Hf. The elementary steps considered and the corresponding energy profiles are depicted in Figures 4 and 5, respectively.

The optimized geometries of the structures involved in the benzyl alcohol dehydrogenation to benzaldehyde (A → C), the competitive benzyl alcohol deprotonation to form an alkoxide (D → E), the condensation of aniline with benzaldehyde (F → G), the dehydration of the resulting intermediate (H → I), and the final hydrogenation of the imine to yield the *N*-benzylaniline product (J → K) are shown in Figures S7 and S8, and the most relevant transition states are depicted in Figure 6.

There are two main modes of adsorption of benzyl alcohol on the Hf Lewis acid sites. The most stable involves the interaction of the hydroxyl group of the alcohol with the Hf center (structure D, Figure 4). Deprotonation of D to produce water and an alkoxide intermediate (structure E) is a reversible process involving an activation energy barrier of only 11.1 kcal/mol (see Figure 5 and Table 2). However, a different orientation of benzyl alcohol is necessary to achieve its dehydrogenation to benzaldehyde. In structure A, the proton of benzyl alcohol hydroxyl group (in red in Figure 4) is stabilized by hydrogen bonding with the basic OH group attached to Hf, leaving the Lewis acid Hf center free to interact

https://doi.org/10.1021/acscatal.1c01739
ACS Catal. 2021, 11, 8049−8061

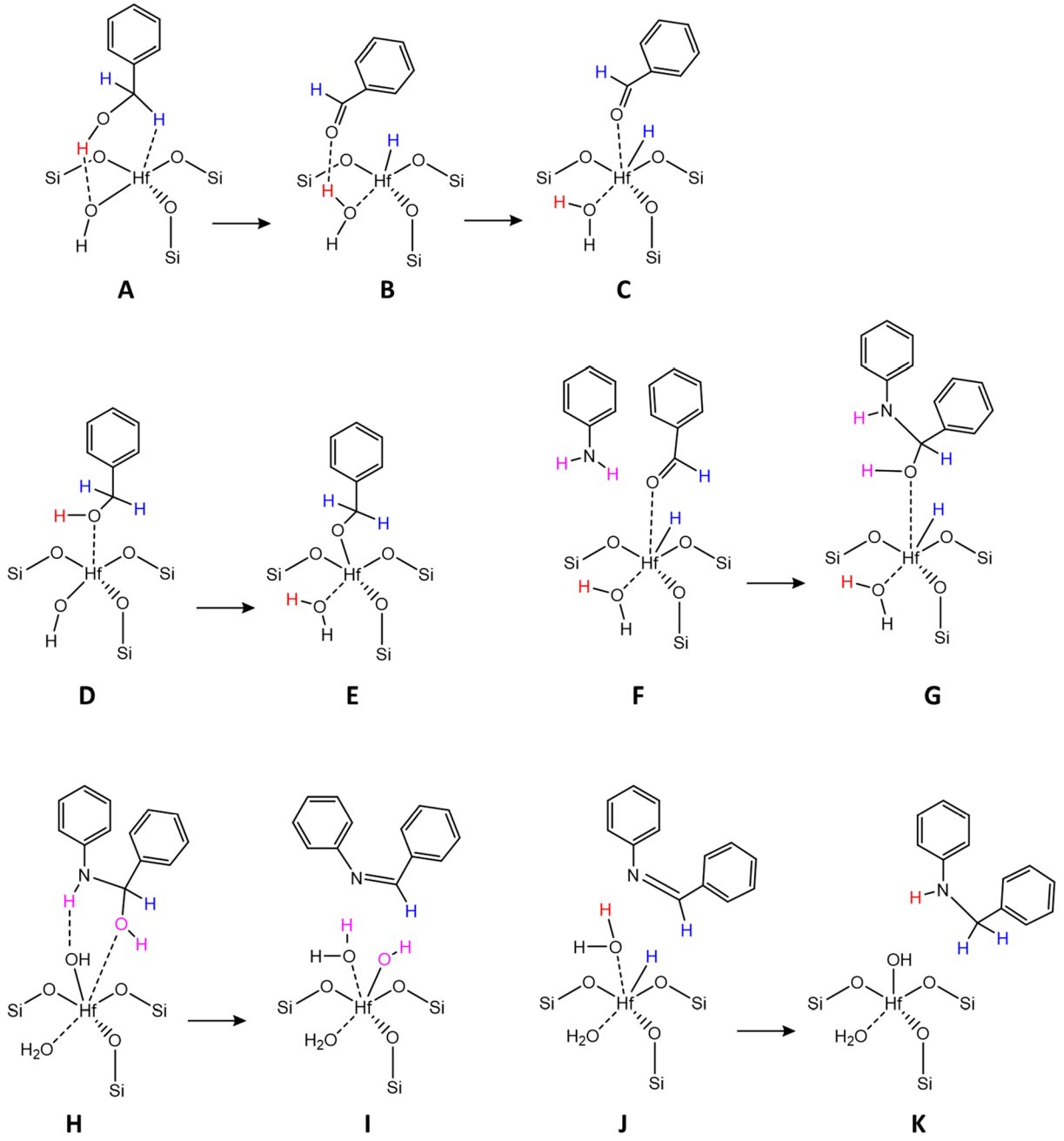

Figure 4. Structures involved in the mechanism of N-alkylation of aniline with benzyl alcohol on an open site model of Hf-Beta zeolite.

with one of the methylene hydrogen atoms (in blue in Figure 4) of benzyl alcohol.

In the transition state TS(AB), the two hydrogen atoms are transferred simultaneously to the catalyst through a six-membered ring (see Figure 6), with an activation energy of 32 kcal/mol (Figure 5 and Table 2). Then, the benzaldehyde molecule obtained evolves from an H-bonded state (structure B) to a more stable system with the carbonyl group clearly interacting with the Lewis acid Hf center (structure C) (see Figures 4 and S7). In this process, the proton of the benzyl alcohol reactant is transferred to the basic hydroxyl group of the open active site to form a neutral water molecule that remains coordinated to Hf, while the methylene hydrogen atom is transferred to Hf as a hydride, as indicated by the Bader net atomic charges summarized in Table 3. So, both basic and redox centers implied in the borrowing hydrogen mechanism are present in the open site of Hf-Beta zeolites. In contrast, the same process on a closed site is thermodynamically unfavorable, because this center lacks the basic OH group (see Figure S9a). On the other hand, while structure D leading to the alkoxide intermediate E is 12 kcal/mol more stable than structure A involved in the dehydrogenation to benzaldehyde, the presence of a water molecule adsorbed on the Hf center stabilizes preferentially the desired mode of adsorption of benzyl alcohol, making both structures similarly stable (see Figure S9b).

Next, aniline adsorbs close to benzaldehyde with the two aromatic rings almost parallel and separated by ~3.5 Å (structure F in Figures 4 and S8). The simultaneous formation of the new C−N bond and the proton transfer from N to O in

https://doi.org/10.1021/acscatal.1c01739
ACS Catal. 2021, 11, 8049−8061

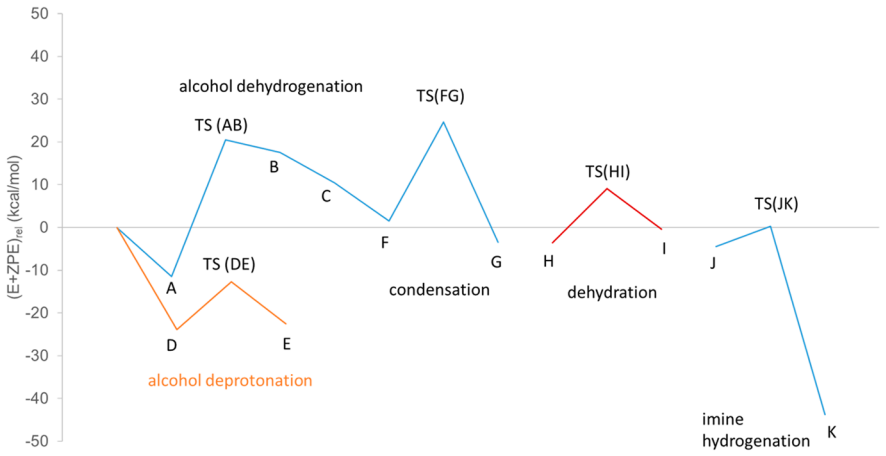

Figure 5. DFT-calculated energy profile corresponding to the N-alkylation of aniline with benzyl alcohol on an open site model of Hf-Beta zeolite. DFT energies include ZPE corrections.

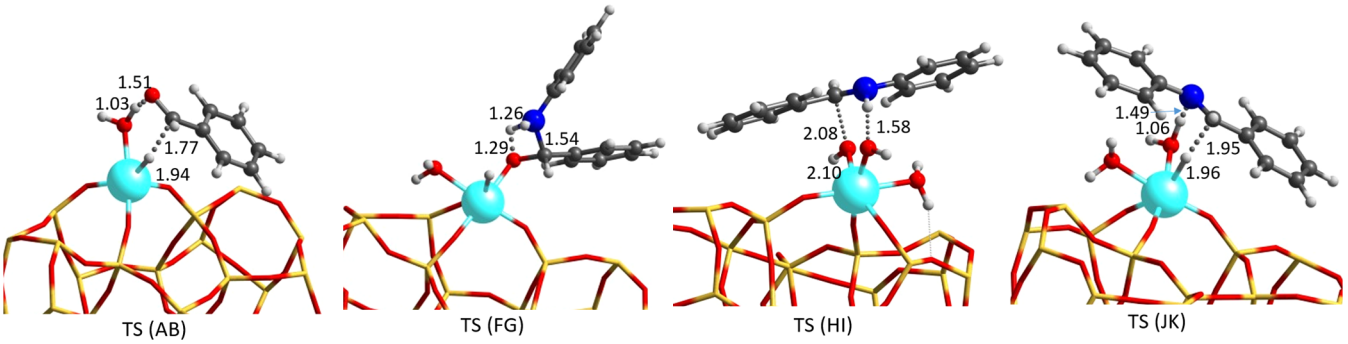

Figure 6. Optimized geometries of the most relevant transition states involved in the mechanism of N-alkylation of aniline with benzyl alcohol on an open site model of Hf-Beta zeolite. Distances in Å. Framework Si and O atoms are depicted as yellow and red sticks. Hf, C, N, H, and O atoms participating in the reaction are depicted as cyan, gray, blue, white, and red balls, respectively.

Table 2. Activation (E_{act}) and Reaction (ΔE) Energies in kcal/mol for All Elementary Steps of the Mechanism of N-Alkylation of Aniline with Benzyl Alcohol on an Open Site Model of Hf-Beta Zeolite[a]

step	labels	E_{act} (kcal/mol)	ΔE (kcal/mol)
alcohol dehydrogenation	A → B → C	32.0	29.1[b]/21.9[c]
alcohol deprotonation	D → E	11.1	1.4
condensation	F → G	23.1	−5.0
dehydration	H → I	12.6	3.2
imine hydrogenation	J → K	4.8	−39.2

[a]DFT energies include a ZPE correction. [b]To structure B. [c]To structure C.

Table 3. Net Atomic Charges on Selected Atoms of Structures A, B, C, and TSAB Involved in the Dehydrogenation of Benzyl Alcohol to Benzaldehyde on the Hf-Beta Catalyst Model

atom	A	TSAB	B	C
Hf	2.309	2.0009	2.009	1.911
O[a]	−1.114	−1.011	−0.988	−0.956
H[a]	0.533	0.546	0.546	0.542
O[b]	−0.783	−0.678	−0.606	−0.581
H[b]	0.518	0.554	0.556	0.546
H[c]	0.207	−0.273	−0.380	−0.367

[a]In the Hf−OH group. [b]In the benzyl alcohol OH group. [c]Methylene hydrogen.

transition state TS(FG) requires an activation energy of 23.1 kcal/mol and produces an intermediate structure (G in Figure 4) 5 kcal/mol more stable than separated reactants (see Table 2). Dehydration of this intermediate to yield the corresponding imine cannot occur directly on the Hf-hydride site but requires its desorption and migration to a different Hf-Beta open site (structure H in Figures 4 and S8). Again, the basic hydroxyl group attached to Hf accepts a proton from N forming water, while the OH group of the organic moiety is transferred to the Hf atom in a concerted way through a cyclic transition state TS(HI) with an activation energy of only 12.6 kcal/mol. Finally, the resulting imine is hydrogenated on the Hf-hydride site through transition state TS(JK) (see Figure 6) with a low barrier of 4.8 kcal/mol, yielding the highly stable *N*-benzylaniline product. In this step, the hydride attacks the C atom of the C=N bond, while the N atom abstracts a proton from the water molecule coordinated to Hf, thus regenerating the initial Hf-Beta open site.

At this point, additional *in situ* IR studies have been performed on the previously described benzaldehyde-adsorbed Hf-Beta sample, which was obtained after exposure to benzyl alcohol at 150 °C for 2 h, evacuation, and cooling down to 100 °C (Figure S10a). After evacuation, aniline has been then coadsorbed (IR bands at 3478, 3385, 1605, and 1500 cm^{-1}), resulting in a fast disappearance of the carbonyl IR band and the formation of water (1622 cm^{-1}) (Figure S10b). After 30

https://doi.org/10.1021/acscatal.1c01739
ACS Catal. 2021, 11, 8049−8061

min at 100 °C, the N−H vibration (IR band at 3426 cm^{-1}) is clearly observed in the IR spectra, with the corresponding disappearance of NH_2 vibration, inferring then the formation of *N*-benzylaniline (Figure S10c).

To support the proposed borrowing hydrogen mechanism (Scheme 2), different deuterium-labeling experiments have been proposed.

Scheme 2. Proposed Mechanism for the N-Alkylation of Aniline with Alcohol Catalyzed by Hf-Beta

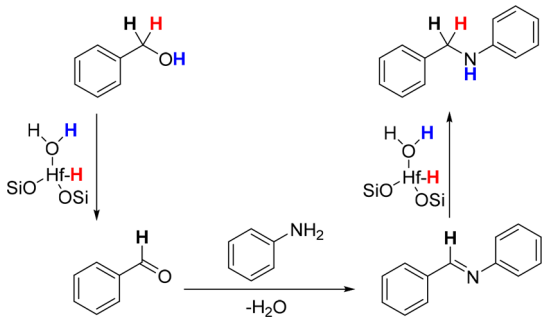

First, the deuterium incorporation in *N*-benzylaniline has been studied starting from isotopically enriched $PhCD_2OH$ and aniline. The product distribution analysis by ^1H NMR spectroscopy shows the selective transformation of the starting materials to fully incorporated deuterium in the methylene position at *N*-benzylaniline **3**-d_2 (see c) in Figure 7). In contrast, the reaction between benzyl alcohol-OD and aniline gave deuterium-free **3** as the major product (see b) in Figure 7), clearly indicating that deuterium incorporation in the methylene position of the *N*-benzylamine product does not proceed from the hydroxyl group of benzyl alcohol.

An additional experiment with subproduct imine **4** as a starting material and benzyl alcohol has also been conducted to evaluate if the proposed borrowing hydrogen mechanism also facilitates the imine hydrogenation with Hf-Beta. The imine hydrogenation with isotopically enriched $PhCD_2OH$ also displays the selective deuterated incorporation in the final amine product. It is worth noting that some fully deuterium incorporation in the methylene position of *N*-benzylaniline product (see c) in Figure 8) would indicate the reversibility of the imine formation. Finally, the imine hydrogenation with $PhCH_2OD$ does not result in the deuterium incorporation from the hydroxyl group in the final *N*-benzylaniline product (see b) in Figure 8), corroborating that the imine hydrogenation occurs through methylene hydrogens from benzyl alcohol.

3.4. Catalyst Regeneration and Substrate Scope. The stability and reusability of the Hf-Beta catalyst have been tested under solvent-free conditions. The catalyst maintains, at least after four consecutive cycles, conversion values above 95% and *N*-benzylaniline selectivities over 90% (see Figure 9). After the fourth evaluation, the catalyst has been recovered by the filtration process and analyzed by powder X-ray diffraction. The crystallographic structure of Hf-Beta is maintained after reuse (see Figure S11).

Other amines and alcohols have been evaluated to expand the substrate scope (Table S2). An aliphatic amine, such as

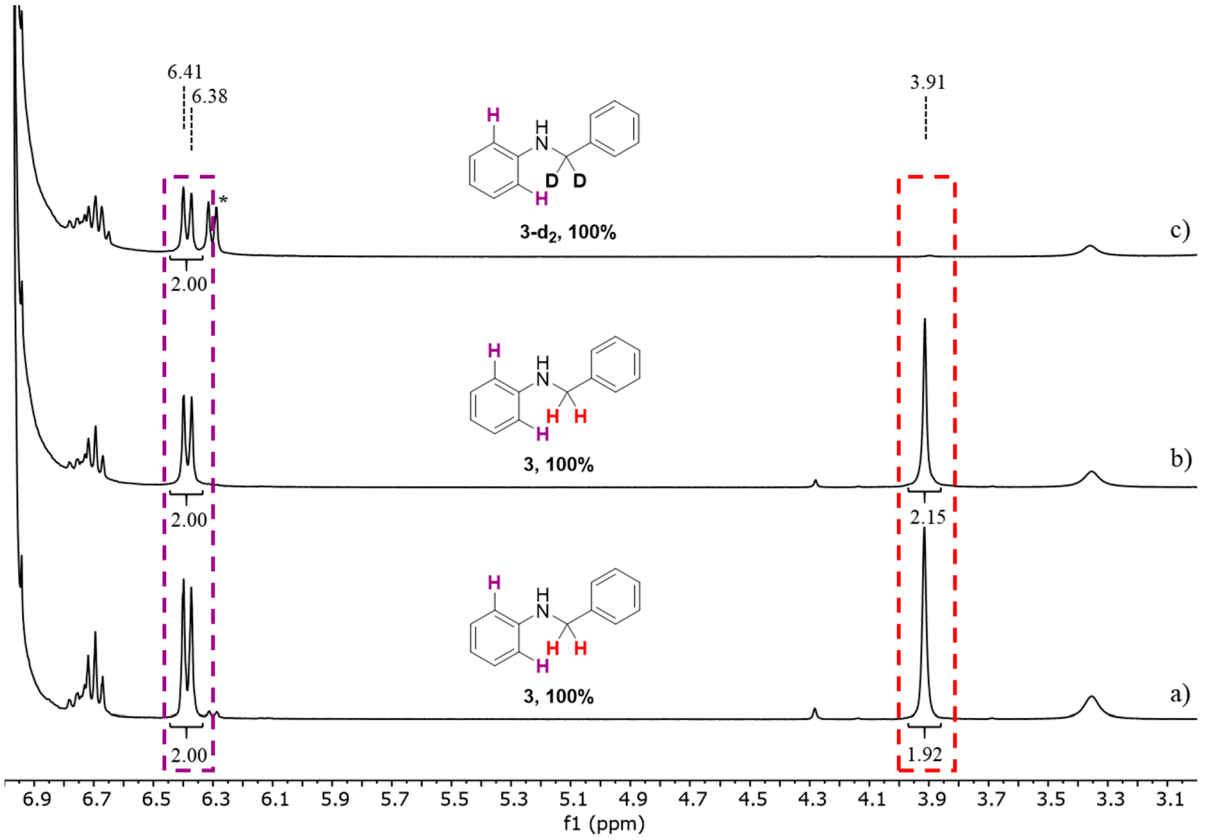

Figure 7. ^1H NMR spectra of the N-alkylation reaction crude of aniline with (a) benzyl alcohol, (b) benzyl alcohol-OD, and (c) benzyl alcohol-α,α-d_2 recorded in toluene-d_8. Asterisk represents a signal of starting aniline without reacting.

https://doi.org/10.1021/acscatal.1c01739
ACS Catal. 2021, 11, 8049−8061

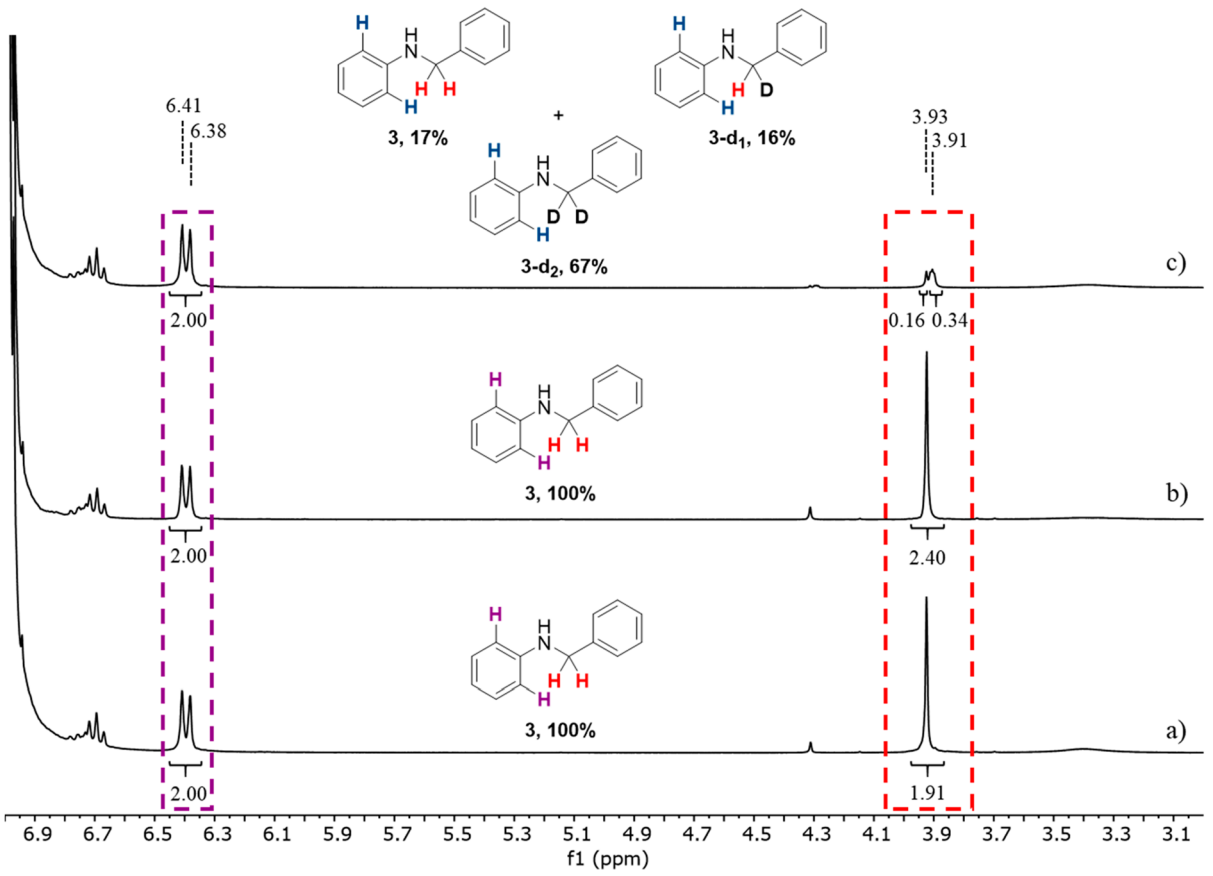

Figure 8. ^{1}H NMR spectra of the *N*-benzylideneaniline imine reaction crude recorded in toluene-d_8 using (a) benzyl alcohol, (b) benzyl alcohol-OD, and (c) benzyl alcohol-α,α-d_2 as reducing agents.

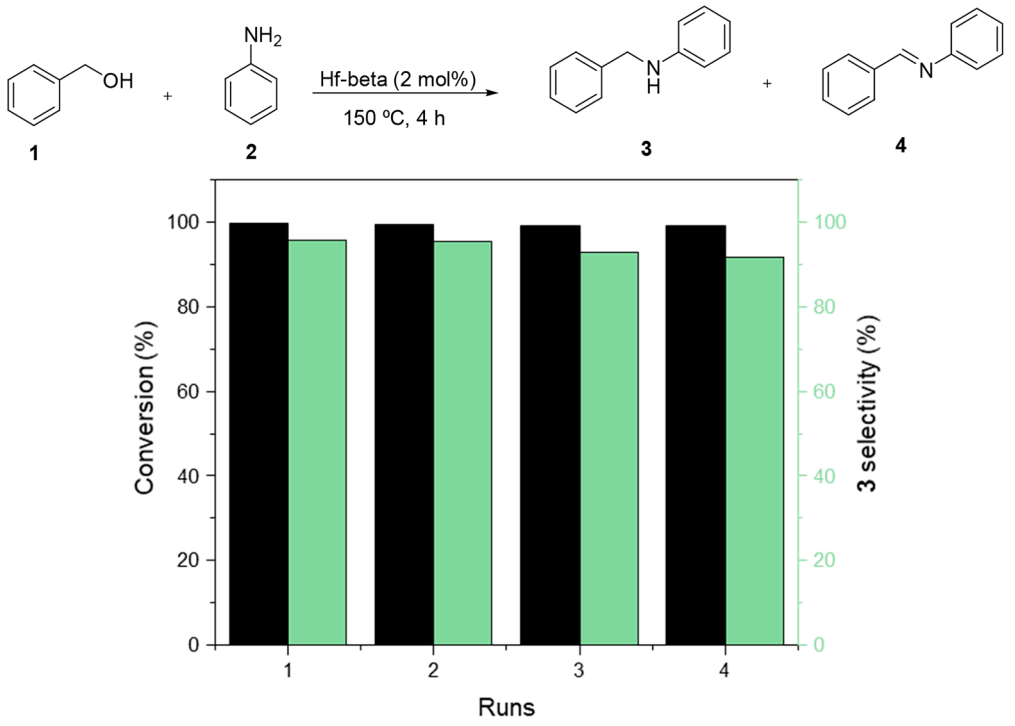

Figure 9. Conversion and **3** selectivity after different recycles using Hf-Beta as a catalyst in the N-alkylation of aniline with benzyl alcohol. Reactions have been run for 4 h after benzyl alcohol activation. Fresh solution was added for each subsequent run.

https://doi.org/10.1021/acscatal.1c01739
ACS Catal. 2021, 11, 8049−8061

butylamine, has been employed in the N-alkylation reaction with benzyl alcohol. Excellent yields toward *N*-benzylbutylamine can be achieved after 24 h (~99%, see Table S2). Biomass-derived amines, such as furfuryl amine, can also be employed to undergo the N-alkylation reaction under similar reaction conditions. Indeed, 95% of amine conversion and 83% of selectivity toward *N*-benzyl-1-(furan-2-yl)methanamine is obtained after 48 h (see Table S2). These results clearly demonstrate that this catalytic system is efficient when using very different amine structures. However, when *n*-butanol has been employed instead of benzyl alcohol as a substrate, only traces of the desired product have been detected after 72 h, indicating that only alcohols with an aromatic ring in the *β*-position can promote the N-alkylation reaction in these conditions when using Lewis-acid-based zeolites as catalysts.

4. CONCLUSIONS

In this work, we have synthesized different Lewis-acid-containing silicates for their application in the N-alkylation tandem reaction of aniline with benzyl alcohol. The materials have been characterized to demonstrate the full incorporation of the Lewis acid sites in the tetrahedral position of the corresponding silicates. The Hf- and Zr-Beta zeolites have shown the highest catalytic activity and selectivity for this transformation. Kinetic studies reveal an induction period observed when using Hf-Beta as catalyst, which could be suppressed by an initial activation with benzyl alcohol. DFT and FTIR analysis indicate that the catalytically active centers for this transformation in Hf-Beta zeolite are the open sites with one hydrolyzed Hf−O bond and that the amount of this type of sites increased considerably when the zeolite was activated with the alcohol. Theoretical and deuterium-labeled experimental studies reveal that the N-alkylation reaction occurs via borrowing hydrogen from the methylene position of the benzyl alcohol substrate, through Hf-hydride intermediates. Finally, Hf-Beta showed high stability after four consecutive runs in this transformation and a diverse substrate scope, including aliphatic and biomass-derived amines.

■ ASSOCIATED CONTENT

Supporting Information

The Supporting Information is available free of charge at https://pubs.acs.org/doi/10.1021/acscatal.1c01739.

Physicochemical properties and characterization of the synthesized M-silicates (PXRD, UV−vis, Raman, FE-SEM); kinetic experiments for N-alkylation of aniline with benzyl alcohol; DFT calculations for the optimized structures of adsorbed acetonitrile in Hf-Beta and reaction intermediates involved in the N-alkylation reaction in Hf-Beta; IR spectra after adsorbing benzyl alcohol in Hf-Beta; and catalytic results for the N-alkylation reaction using different substrates (PDF)

■ AUTHOR INFORMATION

Corresponding Authors

Manuel Moliner − *Instituto de Tecnología Química, Universitat Politècnica de València-Consejo Superior de Investigaciones Científicas, 46022 València, Spain;* orcid.org/0000-0002-5440-716X; Email: mmoliner@itq.upv.es

Mercedes Boronat − *Instituto de Tecnología Química, Universitat Politècnica de València-Consejo Superior de Investigaciones Científicas, 46022 València, Spain;* orcid.org/0000-0002-6211-5888; Email: boronat@itq.upv.es

Authors

Sergio Rojas-Buzo − *Instituto de Tecnología Química, Universitat Politècnica de València-Consejo Superior de Investigaciones Científicas, 46022 València, Spain;* orcid.org/0000-0002-7257-1027

Patricia Concepción − *Instituto de Tecnología Química, Universitat Politècnica de València-Consejo Superior de Investigaciones Científicas, 46022 València, Spain;* orcid.org/0000-0003-2058-3103

Avelino Corma − *Instituto de Tecnología Química, Universitat Politècnica de València-Consejo Superior de Investigaciones Científicas, 46022 València, Spain;* orcid.org/0000-0002-2232-3527

Complete contact information is available at: https://pubs.acs.org/10.1021/acscatal.1c01739

Author Contributions

The manuscript was written through contributions of all authors. All authors have given approval to the final version of the manuscript.

Notes

The authors declare no competing financial interest.

■ ACKNOWLEDGMENTS

This work has been supported by the Spanish Government through "severo Ochoa" (SEV-2016-0683, MINECO), MAT2017-82288-C2-1-P (AEI/FEDER, UE), and RTI2018-101033-B-I00 (MCIU/AEI/FEDER, UE). Dr. Susana Valencia is acknowledged for the preparation of the Ti-Beta sample. The Electron Microscopy Service of the UPV is also acknowledged for their help in sample characterization. Part of the computations were performed on the Tirant III cluster of the Servei d'Informàtica of the University of Valencia.

■ REFERENCES

(1) McGrady, G. S.; Guilera, G. The Multifarious World of Transition Metal Hydrides. *Chem. Soc. Rev.* **2003**, *32* (6), 383−392.

(2) Wilkinson, G.; Birmingham, J. M. Biscyclopentadienylrhenium Hydride—A New Type of Hydride. *J. Am. Chem. Soc.* **1955**, *77* (12), 3421−3422.

(3) Corma, A.; Navas, J.; Sabater, M. J. Advances in One-Pot Synthesis through Borrowing Hydrogen Catalysis. *Chem. Rev.* **2018**, *118* (4), 1410−1459.

(4) Hamid, M. H. S. A.; Allen, C. L.; Lamb, G. W.; Maxwell, A. C.; Maytum, H. C.; Watson, A. J. A.; Williams, J. M. J. Ruthenium-Catalyzed N-Alkylation of Amines and Sulfonamides Using Borrowing Hydrogen Methodology. *J. Am. Chem. Soc.* **2009**, *131* (5), 1766−1774.

(5) Zhang, Y.; Qi, X.; Cui, X.; Shi, F.; Deng, Y. Palladium Catalyzed N-Alkylation of Amines with Alcohols. *Tetrahedron Lett.* **2011**, *52* (12), 1334−1338.

(6) Saidi, O.; Blacker, A. J.; Farah, M. M.; Marsden, S. P.; Williams, J. M. J. Selective Amine Cross-Coupling Using Iridium-Catalyzed "Borrowing Hydrogen" Methodology. *Angew. Chem., Int. Ed.* **2009**, *48* (40), 7375−7378.

(7) Wong, C. M.; Peterson, M. B.; Pernik, I.; McBurney, R. T.; Messerle, B. A. Highly Efficient Rh (I) Homo-and Heterogeneous Catalysts for C−N Couplings via Hydrogen Borrowing. *Inorg. Chem.* **2017**, *56* (23), 14682−14687.

(8) Huang, R.; Yang, Y.; Wang, D.-S.; Zhang, L.; Wang, D. Where Does Au Coordinate to N-(2-Pyridiyl) Benzotriazole: Gold-Catalyzed

Chemoselective Dehydrogenation and Borrowing Hydrogen Reactions. *Org. Chem. Front.* **2018**, *5* (2), 203−209.
(9) Elangovan, S.; Neumann, J.; Sortais, J.-B.; Junge, K.; Darcel, C.; Beller, M. Efficient and Selective N-Alkylation of Amines with Alcohols Catalysed by Manganese Pincer Complexes. *Nat. Commun.* **2016**, *7* (1), 12641.
(10) Rösler, S.; Ertl, M.; Irrgang, T.; Kempe, R. Cobalt-Catalyzed Alkylation of Aromatic Amines by Alcohols. *Angew. Chem., Int. Ed.* **2015**, *54* (50), 15046−15050.
(11) Bains, A. K.; Kundu, A.; Yadav, S.; Adhikari, D. Borrowing Hydrogen-Mediated N-Alkylation Reactions by a Well-Defined Homogeneous Nickel Catalyst. *ACS Catal.* **2019**, *9* (10), 9051−9059.
(12) Yan, T.; Feringa, B. L.; Barta, K. Iron Catalysed Direct Alkylation of Amines with Alcohols. *Nat. Commun.* **2014**, *5* (1), 5602.
(13) Shimizu, K.; Imaiida, N.; Kon, K.; Hakim Siddiki, S. M. A.; Satsuma, A. Heterogeneous Ni Catalysts for N-Alkylation of Amines with Alcohols. *ACS Catal.* **2013**, *3* (5), 998−1005.
(14) Corma, A.; Ródenas, T.; Sabater, M. J. A Bifunctional Pd/MgO Solid Catalyst for the One-Pot Selective N-Monoalkylation of Amines with Alcohols. *Chem. - Eur. J.* **2010**, *16* (1), 254−260.
(15) Corma, A.; Navas, J.; Sabater, M. J. Coupling of Two Multistep Catalytic Cycles for the One-Pot Synthesis of Propargylamines from Alcohols and Primary Amines on a Nanoparticulated Gold Catalyst. *Chem. - Eur. J.* **2012**, *18* (44), 14150−14156.
(16) Wong, C. M.; McBurney, R. T.; Binding, S. C.; Peterson, M. B.; Gonçales, V. R.; Gooding, J. J.; Messerle, B. A. Iridium (Iii) Homo- and Heterogeneous Catalysed Hydrogen Borrowing C−N Bond Formation. *Green Chem.* **2017**, *19* (13), 3142−3151.
(17) Guillena, G.; Ramon, D. J.; Yus, M. Hydrogen Autotransfer in the N-Alkylation of Amines and Related Compounds Using Alcohols and Amines as Electrophiles. *Chem. Rev.* **2010**, *110* (3), 1611−1641.
(18) Schock, L. E.; Marks, T. J. Organometallic Thermochemistry. Metal Hydrocarbyl, Hydride, Halide, Carbonyl, Amide, and Alkoxide Bond Enthalpy Relationships and Their Implications in Pentamethylcyclopentadienyl and Cyclopentadienyl Complexes of Zirconium and Hafnium. *J. Am. Chem. Soc.* **1988**, *110* (23), 7701−7715.
(19) Jordan, R. F. Chemistry of Cationic Dicyclopentadienyl Group 4 Metal-Alky I Complexes. *Adv. Organomet. Chem.* **1991**, *32*, 325−387.
(20) Tosin, G.; Santini, C. C.; Baudouin, A.; De Mallman, A.; Fiddy, S.; Dablemont, C.; Basset, J.-M. Reactivity of Silica-Supported Hafnium Tris-Neopentyl with Dihydrogen: Formation and Characterization of Silica Surface Hafnium Hydrides and Alkyl Hydride. *Organometallics* **2007**, *26* (17), 4118−4127.
(21) Dufaud, V.; Basset, J. Catalytic Hydrogenolysis at Low Temperature and Pressure of Polyethylene and Polypropylene to Diesels or Lower Alkanes by a Zirconium Hydride Supported on Silica-alumina: A Step toward Polyolefin Degradation by the Microscopic Reverse of Ziegler−Natta Pol. *Angew. Chem., Int. Ed.* **1998**, *37* (6), 806−810.
(22) Casty, G. L.; Matturro, M. G.; Myers, G. R.; Reynolds, R. P.; Hall, R. B. Hydrogen/Deuterium Exchange Kinetics by a Silica-Supported Zirconium Hydride Catalyst: Evidence for a σ-Bond Metathesis Mechanism. *Organometallics* **2001**, *20* (11), 2246−2249.
(23) Zakharov, V. A.; Yermakov, Y. I. Supported Organometallic Catalysts for Olefin Polymerization. *Catal. Rev.: Sci. Eng.* **1979**, *19* (1), 67−103.
(24) Zhao, Y.; Truhlar, D. G. The M06 Suite of Density Functionals for Main Group Thermochemistry, Thermochemical Kinetics, Noncovalent Interactions, Excited States, and Transition Elements: Two New Functionals and Systematic Testing of Four M06 Functionals and 12 Other Functionals. *Theor. Chem. Acc.* **2008**, *119* (5−6), 525−525.
(25) Ditchfield, R.; Hehre, W. J.; Pople, J. A. Self-Consistent Molecular-Orbital Methods. IX. An Extended Gaussian-Type Basis for Molecular-Orbital Studies of Organic Molecules. *J. Chem. Phys.* **1971**, *54* (2), 724−728.
(26) Hehre, W. J.; Ditchfield, R.; Pople, J. A. Self—Consistent Molecular Orbital Methods. XII. Further Extensions of Gaussian—Type Basis Sets for Use in Molecular Orbital Studies of Organic Molecules. *J. Chem. Phys.* **1972**, *56* (5), 2257−2261.
(27) Hay, P. J.; Wadt, W. R. Ab Initio Effective Core Potentials for Molecular Calculations. Potentials for K to Au Including the Outermost Core Orbitals. *J. Chem. Phys.* **1985**, *82* (1), 299−310.
(28) Hay, P. J.; Wadt, W. R. Ab Initio Effective Core Potentials for Molecular Calculations. Potentials for the Transition Metal Atoms Sc to Hg. *J. Chem. Phys.* **1985**, *82* (1), 270−283.
(29) Frisch, M. J.; Trucks, G. W.; Schlegel, H. B.; Scuseria, G. E.; Robb, M. A.; Cheeseman, J. R.; Scalmani, G.; Barone, V.; Mennucci, B.; Petersson, G. A.; Nakatsuji, H.; Caricato, M.; Li, X.; Hratchian, H. P.; Izmaylov, A. F.; Bloino, J.; Zheng, G.; Sonnenberg, J. L.; Hada, M.; Ehara, M.; Toyota, K.; Fukuda, R.; Hasegawa, J.; Ishida, M.; Nakajima, T.; Honda, Y.; Kitao, O.; Nakai, H.; Vreven, T.; Montgomery, J. A., Jr.; Peralta, J. E.; Ogliaro, F.; Bearpark, M.; Heyd, J. J.; Brothers, E.; Kudin, K. N.; Staroverov, V. N.; Kobayashi, R.; Normand, J.; Raghavachari, K.; Rendell, A.; Burant, J. C.; Iyengar, S. S.; Tomasi, J.; Cossi, M.; Rega, N.; Millam, J. M.; Klene, M.; Knox, J. E.; Cross, J. B.; Bakken, V.; Adamo, C.; Jaramillo, J.; Gomperts, R.; Stratmann, R. E.; Yazyev, O.; Austin, A. J.; Cammi, R.; Pomelli, C.; Ochterski, J. W.; Martin, R. L.; Morokuma, K.; Zakrzewski, V. G.; Voth, G. A.; Salvador, P.; Dannenberg, J. J.; Dapprich, S.; Daniels, A. D.; Farkas, O.; Foresman, J. B.; Ortiz, J. V.; Cioslowski, J.; Fox, D. J. *Gaussian 09*; Gaussian, Inc.: Wallingford, CT, 2009.
(30) Reed, A. E.; Weinstock, R. B.; Weinhold, F. Natural Population Analysis. *J. Chem. Phys.* **1985**, *83* (2), 735−746.
(31) Alonso, F.; Riente, P.; Yus, M. Alcohols for the α-Alkylation of Methyl Ketones and Indirect Aza-Wittig Reaction Promoted by Nickel Nanoparticles. *Eur. J. Org. Chem.* **2008**, *2008* (29), 4908−4914.
(32) Corma, A.; Nemeth, L. T.; Renz, M.; Valencia, S. Sn-Zeolite Beta as a Heterogeneous Chemoselective Catalyst for Baeyer−Villiger Oxidations. *Nature* **2001**, *412* (6845), 423−425.
(33) Boronat, M.; Concepción, P.; Corma, A.; Renz, M.; Valencia, S. Determination of the Catalytically Active Oxidation Lewis Acid Sites in Sn-Beta Zeolites, and Their Optimisation by the Combination of Theoretical and Experimental Studies. *J. Catal.* **2005**, *234* (1), 111−118.
(34) Boronat, M.; Corma, A.; Renz, M. Mechanism of the Meerwein− Ponndorf− Verley− Oppenauer (MPVO) Redox Equilibrium on Sn− and Zr− Beta Zeolite Catalysts. *J. Phys. Chem. B* **2006**, *110* (42), 21168−21174.
(35) Lewis, J. D.; Van de Vyver, S.; Román-Leshkov, Y. Acid-Base Pairs in Lewis Acidic Zeolites Promote Direct Aldol Reactions by Soft Enolization. *Angew. Chem., Int. Ed.* **2015**, *54* (34), 9835−9838.
(36) Moliner, M. State of the Art of Lewis Acid-Containing Zeolites: Lessons from Fine Chemistry to New Biomass Transformation Processes. *Dalt. Trans.* **2014**, *43* (11), 4197−4208.
(37) Guo, Q.; Sun, K.; Feng, Z.; Li, G.; Guo, M.; Fan, F.; Li, C. A Thorough Investigation of the Active Titanium Species in TS-1 Zeolite by In Situ UV Resonance Raman Spectroscopy. *Chem. - Eur. J.* **2012**, *18* (43), 13854−13860.
(38) Kang, Z.; Zhang, X.; Liu, H.; Qiu, J.; Yeung, K. L. A Rapid Synthesis Route for Sn-Beta Zeolites by Steam-Assisted Conversion and Their Catalytic Performance in Baeyer−Villiger Oxidation. *Chem. Eng. J.* **2013**, *218*, 425−432.
(39) Li, G.; Gao, L.; Sheng, Z.; Zhan, Y.; Zhang, C.; Ju, J.; Zhang, Y.; Tang, Y. A Zr-Al-Beta Zeolite with Open Zr (Iv) Sites: An Efficient Bifunctional Lewis−Brønsted Acid Catalyst for a Cascade Reaction. *Catal. Sci. Technol.* **2019**, *9* (15), 4055−4065.
(40) Zhao, Z.; Liu, Y.; Wu, H.; Li, X.; He, M.; Wu, P. Hydrothermal Synthesis of Mesoporous Zirconosilicate with Enhanced Textural and Catalytic Properties with the Aid of Amphiphilic Organosilane. *Microporous Mesoporous Mater.* **2009**, *123* (1−3), 324−330.
(41) Juarez, R.; Padilla, A.; Corma, A.; Garcia, H. Transition Metal Containing Zeolites and Mesoporous MCM-41 as Heterogeneous Catalysts for the N-Alkylation of 2, 4-Diaminotoluene with Dimethylcarbonate. *Catal. Commun.* **2009**, *10* (5), 472−476.

https://doi.org/10.1021/acscatal.1c01739
ACS Catal. 2021, 11, 8049−8061

(42) Yang, G.; Zhou, L.; Han, X. Lewis and Brönsted Acidic Sites in M4+-Doped Zeolites (M = Ti, Zr, Ge, Sn, Pb) as Well as Interactions with Probe Molecules: A DFT Study. *J. Mol. Catal. A: Chem.* **2012**, *363*−*364*, 371−379.
(43) Botti, L.; Kondrat, S. A.; Navar, R.; Padovan, D.; Martinez-Espin, J. S.; Meier, S.; Hammond, C. Solvent-Activated Hafnium-Containing Zeolites Enable Selective and Continuous Glucose−Fructose Isomerisation. *Angew. Chem., Int. Ed.* **2020**, *59* (45), 20017−20023.
(44) Bukowski, B. C.; Bates, J. S.; Gounder, R.; Greeley, J. First Principles, Microkinetic, and Experimental Analysis of Lewis Acid Site Speciation during Ethanol Dehydration on Sn-Beta Zeolites. *J. Catal.* **2018**, *365*, 261−276.
(45) Rodríguez-Fernández, A.; Di Iorio, J. R.; Paris, C.; Boronat, M.; Corma, A.; Román-Leshkov, Y.; Moliner, M. Selective Active Site Placement in Lewis Acid Zeolites and Implications for Catalysis of Oxygenated Compounds. *Chem. Sci.* **2020**, *11* (37), 10225−10235.

https://doi.org/10.1021/acscatal.1c01739
ACS Catal. 2021, 11, 8049−8061